Thermal behaviour modelling of a reference calorimeter for natural gas

Frédérique Haloua [a,*], Jean-Noël Ponsard [b], Ghislain Lartigue [b], Bruno Hay [a], Clotilde Villermaux [b], Emilie Foulon [a], Murès Zaréa [b]

[a] Materials Department, Photonics and Energy Division, Scientific and Industrial Metrology Centre, Laboratoire National de Métrologie et d'Essais (LNE), 1 rue Gaston Boissier, 75724 PARIS Cedex 15, France
[b] GDF-SUEZ, R&D Division, BP 33, 93211 St Denis La Plaine Cedex, France

ARTICLE INFO

ABSTRACT

The French National Metrology and Testing Institute (LNE) build an isoperibolic reference gas calorimeter to measure the calorific value of natural gas with a high level of accuracy with the collaboration of the R&D Division of GDF-Suez. With 3D numerical modelling tools, GDF-Suez developed a comprehensive and refined model of the complete calorimeter geometry and evaluated the heat flux sources to reproduce the thermal behaviour of this calorimeter. The objectives are to optimise the thermal homogeneity and to maximize heat transfer to the water bath. The accurate assessment of the different thermal fluxes transferred to the water bath was performed based on a complete simulation of the combustion of the fuel gas in the burner. The numerical model results fit quite closely the experimental thermal behaviour of the calorimeter. The energy balance shows that approximately 90% of the total energy is absorbed by the water bath and about 10% by the calorimetric walls with a weak contribution of the radiative heat transfer to the calorimeter vessel. A comparative study between the numerical and experimental results confirms both that the geometries of the calorimeter vessels and the glass burner are adequate. The new refined geometric model validates also the location of the thermal sensor in the bath. The expected outcome of both experiments and thermal modelling is to decrease the uncertainty of the calorific value measured with this standard combustion calorimeter.

1. Introduction

The European gas market context (wide deregulation since July 1st, 2007) has led gas selling companies to better control cost of the transported and distributed gas, by supervising its energy performance. By invoicing the gas transactions in energy units, the calorific value (quantity of energy released by a complete combustion of a volume, molar or mass unit of a gas) of natural gas has to be precisely determined in order to realistically reflect the energy content of natural gas. Taking into account the volume of gas traded and the financial amount at stake, it is necessary to find out with very low uncertainties the energy content of the components of natural gas.

The calorific value of a natural gas is currently estimated (at gas network sites or in labs) by gas chromatography (indirect method) from the determination of its composition for eleven simple gases of known calorific values (CV). The calorific values given in the ISO 6976 standard [1] result from measurements carried out from the 1930's to the 1970's [2–6] and are not provided with associated uncertainties. The experimental procedure used at that time is not well documented, so the uncertainty budget is incomplete. As currently gas compositions vary due to diversified gas sources, it is crucial to update the above-mentioned data used in the standard, by generating the CV data for all gas components with the associated uncertainties.

Consequently, the Groupe Européen de Recherches Gazières (GERG) began in the early 2000's the development of a combustion reference calorimeter for natural gas allowing direct measurements of CV with an uncertainty target of ±0.05%. Partner in the GERG project, LNE launched a parallel project to set up and characterise another reference gas calorimeter to measure calorific values of pure gases and natural or synthetic gas mixtures.

The French calorimeter was developed at LNE, with a specific modelling contribution of GDF-Suez's R&D Division with the aim

* Corresponding author. 29 avenue Roger Hennequin, 78197 Trappes Cedex, France. Tel.: +33 1 30 69 32 57; fax: +33 1 30 69 12 34.
  E-mail addresses: frederique.haloua@lne.fr (F. Haloua), jean-noel.ponsard@edf.fr (J.-N. Ponsard), ghislain.lartigue@coria.fr (G. Lartigue), bruno.hay@lne.fr (B. Hay), clotilde.villermaux@gdfsuez.com (C. Villermaux), emilie.foulon@lne.fr (E. Foulon), mures.zarea@gdfsuez.com (M. Zaréa).

of optimising the calorimeter design and improving its accuracy. New results of numerical simulations from GDF-Suez are presented here with a more realistic computational model than before [7,8] including combustion modelling in the burner.

This international metrological requirement for energy measurement strongly suggests the need for several standard combustion calorimeters for direct CV measurements of fuel gases. The French reference gas calorimeter was optimised with technical adaptations evidenced by numerical simulations from GDF-Suez aimed at maximizing heat transfer to the calorimetric coolant flow and at improving thermal homogeneity.

Both experimental and numerical water bath temperatures as a function of time during electrical heating and combustion of methane are presented here and a comparative study is exposed.

2. Objectives

During the development at LNE of the reference calorimeter, it was found that CV measurements and uncertainty calculations are strongly dependent on thermal effects occurring in the calorimeter during experiments and more specifically on the thermal homogeneity and heat transfer quality.

GDF-Suez performed detailed transient 3D numerical simulations of the flow and heat transfer in the calorimeter water bath in order to optimise the thermal homogeneity and maximize heat transfer from heating sources (combustion or electrical heating) to the water bath. The numerical results presented here are obtained with a refined computational dynamic model that integrates:

- A more realistic accounting for some complex geometrical aspects of the calorimeter
- High accuracy steady state combustion modelling of the burner.

The main objectives of the study consist in:

- Understanding the thermal behaviour of the calorimetric water bath in terms of heat transfers mechanisms during heating (electrical and combustion),
- Comparing the time evolution of temperature curves from experimental and numerical results in both electrical and combustion modes,
- Assessing the analogy between electrical and combustion modes as well as validating both the temperature sensor location in the calorimetric water bath and the jacket temperature level.

3. Operating principle of the reference calorimeter

After studying various calorimetric techniques, the isoperibolic principle was adopted. The direct method with an isoperibolic reference gas calorimeter can perform gross calorific value (GCV) measurements with the lowest possible uncertainty. *Gross* calorific value differs from *net* calorific value by the state of the water produced by the combustion: gross for liquid state and net for the gaseous (vapour) state of the water.

The French reference calorimeter for natural gas consists in a glass burner in which a given quantity of methane is burnt (Fig. 1) [9]. The heat released during combustion is transmitted to a water volume that surrounds the burner. The calorimetric vessel is thermally uncoupled from outside by the means of an enclosure maintained at 25 °C that characterizes the isoperibolic aspect. This temperature was optimised after a numerical study of the water
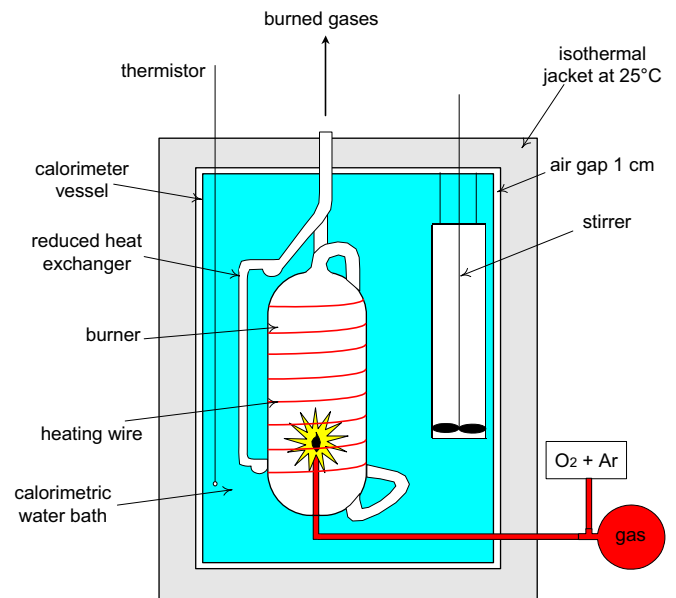

Fig. 1. Schematic of the LNE reference combustion calorimeter with the glass burner.

bath temperature in the electrical heating case where two jacket temperatures were tested (results exposed in section 5.4).

The calculation of the water temperature rise in an ideal adiabatic case ΔT_{ad} resulting from the raw temperature data allows an evaluation of GCV according to Eq. (1):

$$GCV = \frac{C_{cal}\Delta T_{ad} + K}{m_{gas}} \tag{1}$$

Where C_{cal} (J K^{-1}) is the heat capacity of the calorimeter determined by electrical calibration, ΔT_{ad} (°C) is the calculated calorimeter water bath temperature rise issued from the heat released during combustion in an ideal adiabatic case, K (J) represents the different energy corrections (ignition energy, energy due to water vapour leaving the calorimeter, energy due to temperature differences between in - and out - flowing gases) and m_{gas} (g) is the burnt mass of methane.

The burnt gases circulate in a reduced heat exchanger (Fig. 1) and leave the calorimeter for gas analyses of unburnt CH_4, CO and CO_2 components. The mass of the fuel gas, initially contained in a pressurized sphere at 18 bars, is determined by the double weighing method with a mass comparator adapted for this purpose. The heat capacity of the calorimeter C_{cal} is determined by electrical calibration with a heating wire coiled around the burner wall (red wire in Fig. 1) that provides Joule effect dissipation with a power of ∼46 W that simulates as close as possible the combustion heat release. A thermistor of 10 kΩ resistance was chosen to follow the bath temperature for its high sensitivity (430 Ω/°C), small geometry (1 mm diameter of the bead) and fast response time (1.5 s in an oil bath) [8,10].

Fig. 2 shows a typical water bath temperature time curve (combustion or electrical calibration). Calibration and combustion experiments consist in three periods of 20 min each: two quasi-stable phases during which the calorimetric water bath only supports continuous stirring (also called the initial and the final period) and the main period of heat input (stirring always occurs) by electric or combustion way and during which the mean bath temperature experiences the main rise. T_j is the temperature of the jacket maintained at 25 °C. This chosen temperature represents the standard temperature of combustion for GCV measurements issued
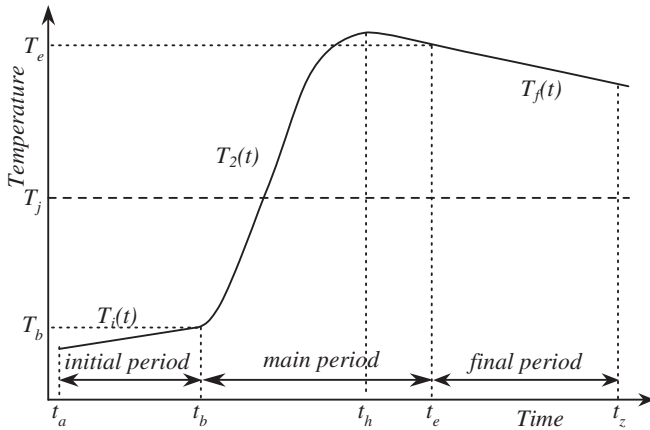
Fig. 2. Temperature-time curve scheme for an isoperibolic calorimeter.

Fig. 3. Representation of the flame at the exit of the injector and incoming gas reactants in the burner.

from the ISO 6976 standard [1]. In an effort to comply as closely as possible the standard combustion temperature, measurements of the water bath temperatures surround this value. Validation of T_j is presented in part 5.

Previous transient 3D numerical simulations of the flow and heat transfer in the calorimetric water bath [7,8,11] during stable phases (no heat release) and heating periods showed similar temperature evolutions for experimental and numerical results in combustion (pure radiative heat transfer) and calibration (imposed surface flux case) modes. In particular, the design of the calorimeter vessels and the location of the thermistor chosen by LNE were validated. The sensor position between the burner and the vessel wall at the opposite side of the stirrer represented the optimised site for water bath mean temperature measurements.

Nevertheless, the Computational Fluid Dynamics (CFD) thermal model using ANSYS-CFX© software had identified items to be clarified, as differences in the thermal fields in calibration and combustion modes. A more realistic and accurate model was needed, particularly in the combustion mode.

4. Implementation of a new computational set up

Improvements were brought to the initial transient 3D numerical simulation [11] by refining the modelling [12]. Special attention was paid to the combustion mode:

- Advanced chemistry steady state modelling of the combustion in the burner
- Comprehensive representation of a new burner geometry including its thermal inertia due to its thickness.

4.1. Modelling of the combustion in the burner

The combustion mode simulation required the modelling of the combustion in the burner in order to know the different heat flux entering the water bath. The combustion in the burner presents a particular mode that was unusual to predict. Indeed, two different inflowing streams of oxygen result in a both premixed (primary O_2, Ar and CH_4 flowing through the injector) and diffusion flame (secondary O_2 flowing around the injector) (Fig. 3). The reactants gas flows are 0.0042 Nm^3/h for CH_4, 0.0027 and 0.0168 Nm^3/h for respectively primary and secondary oxygen and 0.0021 Nm^3/h for Argon.

The combustion in the burner was predicted via the FPI model [13] as Flamelet Prolongation of ILDM (Intrinsic low-dimensional manifold), developed in partnership by GDF-Suez and the EM2C
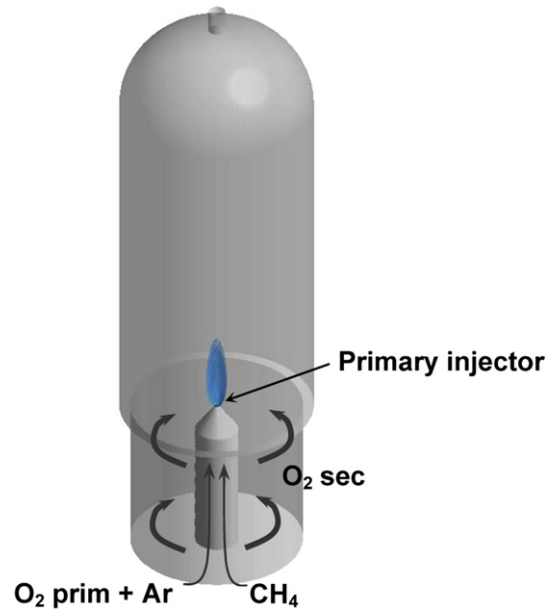
laboratory (Ecole Centrale Paris). This method allows the integration of complex flame kinetics patterns with reference flame calculations and thereafter their incorporation in the CFD calculation. An accurate quantification of the heat release from the flame and of the exhaust gases temperature rise is possible.

An FPI look up table is constructed to store all chemical information, with three coordinates: Y_c a progress variable of the global reaction, Z a mixture fraction characterising the equivalence ratio, and h the enthalpy. Y_c and Z are both suitable combinations of species mass fraction. The coordinate h enables to take account heat losses on the thermochemical data. Thanks to 1D premixed flame calculation, all chemical species involved in the detailed kinetics scheme, the temperature and the thermo chemical data are tabulated in terms of the three coordinates (Y_c, Z, h). Y_c, Z and h are considered as independent variables. It is then possible to construct a turbulent look up table assuming a Beta shaped probability density function (PDF) for Y_c and Z, and a Dirac PDF for the enthalpy. All mean quantities φ needed for the CFD are then stored in a turbulent look up table as followed:

$$\tilde{\varphi} = \tilde{\varphi}\left(\tilde{Y}_c, \widetilde{Y_c''^2}, \tilde{Z}, \widetilde{Z''^2}\right)$$

This tabulation appears as an interesting tool to perform very fast calculations including complexes chemistry effects. In addition to the classical mass, momentum, mean mixture fraction and mixture fraction fluctuations, energy and RANS k-ε balance equations, transport equations for mean progress variable and progress variable fluctuations need to be solved:

$$\frac{\partial \overline{\rho}\tilde{Y}_c}{\partial t} + \nabla \cdot \left(\overline{\rho}\tilde{u}\tilde{Y}_c\right) = \nabla \cdot \left(\frac{\mu_t}{\sigma}\nabla\tilde{Y}_c\right) + \bar{\dot{\omega}}_{Y_c} \frac{\partial \overline{\rho}\widetilde{Y_c''^2}}{\partial t} + \nabla \cdot \left(\overline{\rho}\tilde{u}\widetilde{Y_c''^2}\right)$$

$$= \nabla \cdot \left(\left(\overline{\rho}D + \frac{\mu_t}{\sigma}\right)\nabla\widetilde{Y_c''^2}\right) + 2\frac{\mu_t}{\sigma}\left|\nabla\tilde{Y}_c\right|^2 - 2\overline{\rho D|\nabla Y_c''|^2} + 2\overline{Y_c''\dot{\omega}}_{Y_c}$$

Where μ_t is the turbulent eddy viscosity and $\sigma = 0,6$ is the turbulent Schmidt number. The chemical source terms are pre-stored in the FPI table. The third term of the progress variable fluctuation transport equation is modelled with a linear relaxation
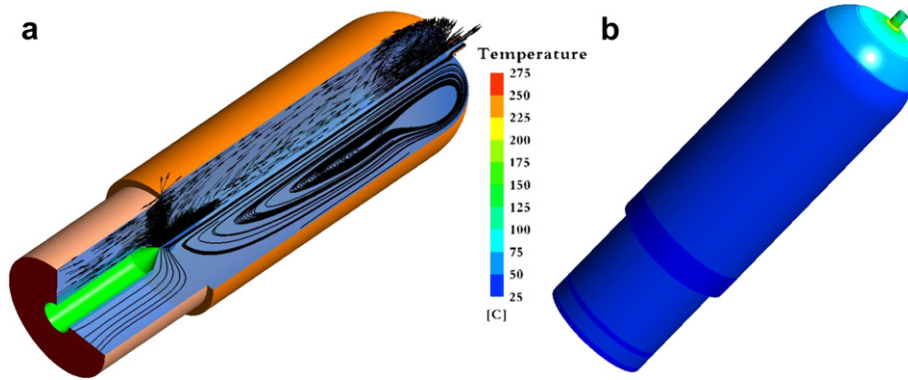
Fig. 4. (a) Streamlines and speed vectors direction of the flow in the burner during combustion. (b) Temperature field at walls with a thermal resistance.

assumption [13]. In the current application, very accurate predictions of temperature and minor species fields are necessary. The FPI model combines these features with a low computational cost. For example, standard model could have overestimated the temperature field/peak and then the temperature field in the water would not have been well predicted.

Even if 70% of the total flow is coming from the secondary oxygen, the surfaces of both injectors (0,2 mm^2 for primary injector and 1178 mm^2 for secondary injector) lead to higher gas speeds from the primary injector (15 m/s) than from secondary injector (5 mm/s). Consequently, flow aerodynamics is mainly managed by the gas jet from the primary injector. The result is a particular stream gas that can be observed in Fig. 4(a) that exposes streamlines and speed vectors direction of the flow. The central jet follows the burner axis and directly exits whereas the dome of the burner recirculates other burned gases.

In addition, it can be observed that the central jet composed of CH_4, Ar and O_2, drags a large amount of gas that is either secondary O_2 flowing around the primary injector or cold burned gases coming from the recirculation zone along the walls (H_2O and CO_2 cooled by the water bath). These gases, mixed together, modify the combustion.

A temperature limit condition was imposed on burner walls by using a thermal resistance law in order to quantify the heat transfer quality through the glass walls of the dome and to make heat exchanges with the water bath consistent. The modelling of heat flux between the hot gases and the water bath through the glass walls is defined as $\Phi = h_{eq}. (T_{gas} - T_{WB})$ where h_{eq} is the heat transfer coefficient, T_{gas} and T_{WB} are respectively the gas and the water bath temperatures. Conduction and convection heat transfer modes are taken into account in the h_{eq} determination.

The heat transfer coefficient h_{eq} can be expressed with the following equation with e the wall combustion chamber thickness, λ its thermal conductivity and h_{WB} the water bath convective heat

transfer coefficient estimated via the correlation for flat plate given by [14]:

$$\frac{1}{h_{eq}} = \frac{e}{\lambda} + \frac{1}{h_{WB}}$$

Calculations show that the temperature field to the wall is of 25 °C, which means that heat exchanges are very important at the walls. Fig. 4(b) presents temperature field to the wall in the case of simulation with a thermal resistance law. It is observed that the walls temperature reaches maximum 275 °C at the junction between the dome and the coil. However, this zone is very reduced, and only the top of the dome presents temperatures above 50 °C. Heat transfers at this location are then very important and the water around this site is heated more rapidly than the water elsewhere. Consequently, water temperature picks are waited locally at this site. An experimental validation of this numerical result will be exposed later.

Thus, the burned gases are very quickly cooled by the water bath when they come into contact with the walls of the dome.

Considering these results, it has been decided to drastically reduce the heat exchanger (initially a glass coil around the burner [10]) to one half turn (see Fig. 5). Two little water traps have been added in order to collect water produced by the combustion and to keep it in the calorimeter as liquid to reach as much as possible the gross calorific value (water produced by combustion must remain as liquid).

It has also been demonstrated that the radiation of burned gases is weak in large wavelengths. As the fumes in the burner are quickly cooled (validated by outflowing gas temperature measurements during combustion with a platinum sensor 100 Ω) and glass and water are considered as opaque materials, the weak flame radiance and the radiative heat transfer of burned gases are rapidly absorbed within a thickness of 5 mm of water in the bath. These results allow
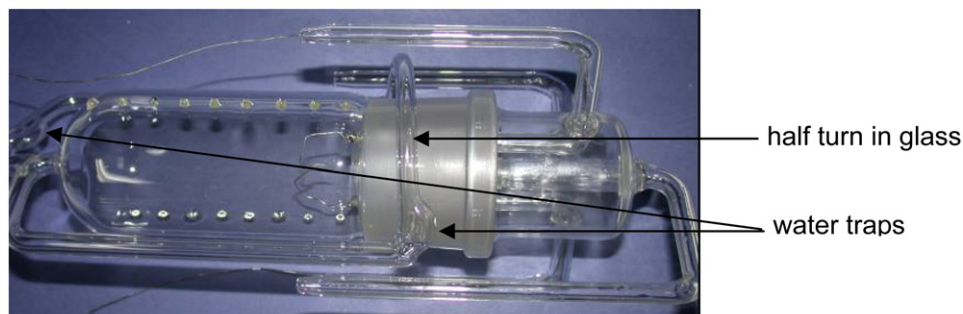

Fig. 5. New burner with reduced heat exchanger and two water traps.

the numerical simulation of the water bath behaviour in the combustion mode without radiation.

4.2. Refined geometric model applied in combustion and calibration modes

The modelled volume corresponds to the water bath stirred in the calorimeter. It includes the burner walls with its thickness, the reduced heat exchanger, all the accessories (the volume of the four pipes, the cooling finger, the stirrer axis, the temperature sensors and the recirculating channel) and the walls of the calorimeter vessels. Fig. 6 exposes the geometric model realized by GDF-Suez R&D division.

The walls of the calorimeter cans are here separated in three layers (two layers in stainless steel and one in air) in order to be precisely representative of the different heat transfers existing between these layers. The stirring is initiated by a momentum source in the recirculating channel and is adjusted to obtain a water flow of 30 cm s^{-1} at the bottom exit of the channel. This water flow was empirically determined in order to obtain good stirring of the water bath without vortex phenomenon at the top of the channel. Total water volume is approximately 4.2 l in the inner can.

The whole geometry is modelled in a large hybrid mesh, non structured for the water volume and structured for the rest. The total mesh consists of 782 000 elements and 400 000 nodes.

5. Results and discussion

In both modes (combustion and calibration), the thermal power released is around 46.54 W during 20 min that corresponds to an amount of energy of 55 836 J. The main difference between the two modes lies in the distribution of the energy load. In the calibration mode, heat is uniformly applied along the burner surface on 10 cm height with the heating wire (Fig. 1). Modelling of the distribution of the total power released during combustion (in the heat exchanger and in the burner with condensed water) was also
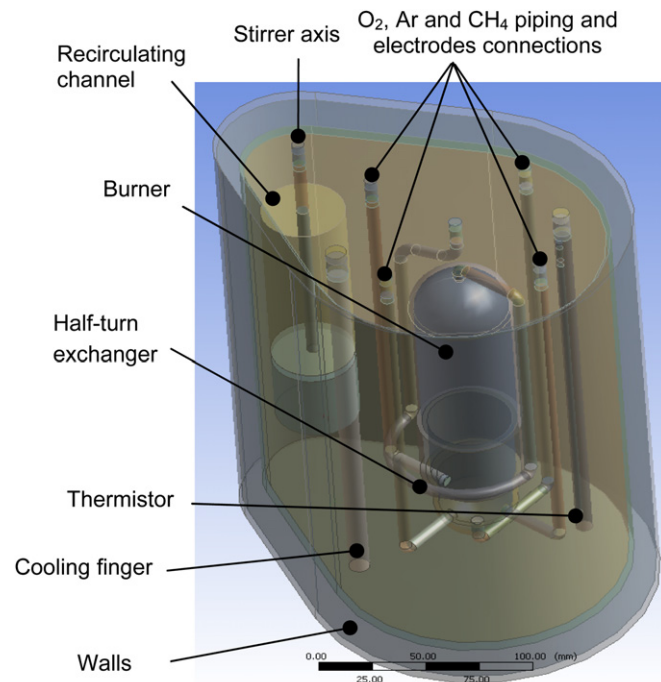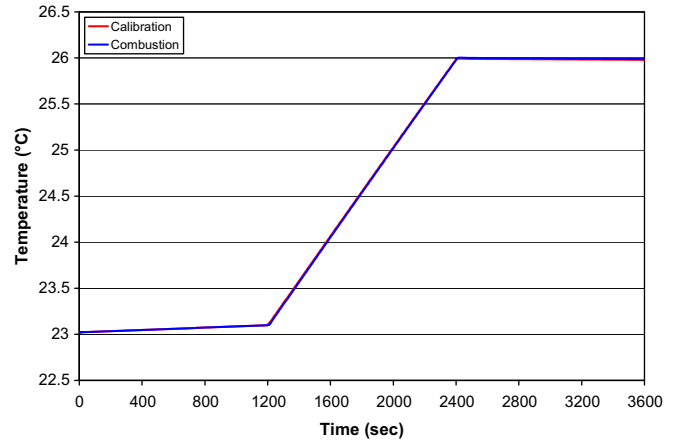
Fig. 7. Evolution of the simulated mean water bath temperature for calibration and combustion.

possible with realistic hypotheses based on experimental [15] and modelling results (combustion in the burner and cooling coil modelled).

Consequently, 39.95 W of the total thermal power is applied as convective flux at the burner walls, 1.8 W in the reduced heat exchanger and 4.79 W through condensed thermal heat flux in the upper part of the burner.

Results exposed here are mainly focused on temperature evolutions of the thermistor located at a special site in the bath [7] and representative of the mean water bath temperature. Results of the comparison between new experimental results issued from thermal characterisation of the calorimetric water bath during transient periods (combustion and electrical calibration) and numerical results in the same configuration obtained with the new refined model are presented and described below. They validate both the improved thermal model used and applied to this particular and unusual combustion mode and also the position of the thermistor in the bath. In addition, numerical results confirmed the jacket temperature level.

5.1. Simulated results

5.1.1. Calibration vs. combustion

First general result from numerical simulations concerns the analogy of the thermal behaviour between the two modes. Fig. 7 presents the evolution of the water bath mean temperature in

Fig. 6. Refined geometric model.

Table 1
Simulated energetic distribution during the main (heating) and final periods in calibration and combustion for the main elements of the calorimeter.

	Calorimetric element	Energy absorbed during calibration (J)	Energy absorbed during combustion (J)
Main period	Burner (glass) walls	613	926
	Internal calorimetric walls	4857	4858
	Calorimetric water bath	50882	50747
	Total	**56352**	**56531**
Final period	Burner (glass) walls	−178	−489
	Internal calorimetric walls	161	180
	Calorimetric water bath	−199	84
	Total	**−216**	**−225**

Table 2
Comparison results on times t_e and t_{Tmax} resulting from experiments and simulations in both calibration and combustion modes.

		Calibration (sec)	Combustion (sec)
t_e	Modelling	130	140
	Experiment	50	155
t_{Tmax}	Modelling	12	28
	Experiment	14	34

combustion and calibration with the same input data as initial temperature of the bath and the duration of the different periods. The two curves are identical and this points out that both heating modes provide the same behaviour in the water calorimetric bath.

5.1.2. The energetic balance in combustion and calibration

The distribution of the total thermal power absorbed by the calorimetric elements is dependent on the domain, its material and time. Table 1 proposed here the numerical energetic balance for combustion and calibration for each main element constituting the calorimeter and during the main heating period. As the environment is identical during the initial period for both modes where only stirring is applied, the main and final periods are only here considered.

For both modes, the total amount of energy is greater than the heating power applied to the system (55 836 J) because some external heat flux are absorbed by the calorimeter as the energy of stirring or the energy exchanged between the isothermal jacket and the calorimeter walls.

The main information to be used from this table is the major part of energy absorbed by the water bath, whatever the mode applied: 90.3% in the calibration mode and 89.8% in the combustion mode. During the heating periods, the glass walls of the burner directly stored a minor part of energy (613 J for the calibration mode and 926 J for the combustion mode). This stored energy allows the glass to heat to a temperature higher than the water bath. At the beginning of the final period, due to the inertia of the glass, this energy is released to the water because of the temperature difference: −178 J for the calibration mode and −489 J for the combustion mode. The radiative heat transfer from the flame caused the difference between the two modes.

5.2. Comparison between numerical simulations and experiments

Time of completion of heat transfer between the burner and the water bath called t_e (visualized in Fig. 2) and time corresponding to the maximum temperature of the water bath (t_{Tmax}) were calculated by simulations and issued from experiments with

temperature data treatment [9]. Table 2 exposes the comparison between experiments and numerical results of these times, obtained relatively to the time of completion of heat input (t_h in Fig. 2).

Experimental time t_e has been determined from time-temperature curves in both modes through a post-treatment program written in MATLAB® language at LNE. Time t_e is calculated from a step by step linear regression procedure of the final period data points [16]. Experimental time of completion of heat input t_h for combustion was estimated according to the CO concentration peak from burned gases analysis taking into account the response time of the device. In effect, after methane supply is cut off at the end of the main period, a short period of bad combustion occurs (too poor mixture) accompanied by a rapidly increase of CO concentration in the burned gases.

On the whole, the results obtained by the means of simulations and presented in Table 2 correctly reproduce the thermal water bath behaviour during heat transfers. Time t_{Tmax} differs only of few seconds between simulations and experiments (2 s for calibration and 6 s for combustion). A larger difference is observed for time t_e in combustion (15 s) that may be due to an actual greater inertia of the burner glass or shorter time response of the CO analyser. One bigger difference of 80 s between experimental and numerical data concerns time t_e in the calibration mode. After the heating period, the heat release to the water bath is almost completed and the remaining energy (178 J from the glass walls) seems to be experimentally transferred to the bath very rapidly.

Comparison of the bath temperatures evolutions during transient's periods in simulation and experiment is a good validation indicator of the numerical simulations. Following figures expose the mean water bath temperatures in a function of time for both calibration (Fig. 8a) and combustion (Fig. 8b) modes. In a general way, the overall aspect of the numerical simulation curves respect the experimental curves obtained for combustion and electrical heating.

Nevertheless, some slight differences can be observed and hypothetic causes might be identified:

- The slopes of the stabilization periods (initial and final periods) are more important in the experimental case whatever the heating mode: greater heat transfer with the environment (jacket bath) maintained at 25 °C can lead to these differences
- The temperature rise during heating period by combustion (Fig. 8b) is greater than the simulated curve. It can be explained by the combustion model taken into account for the simulations where, as it has been stated above (part 4.1.), the weak contribution of radiative heat transfer by the burned gases was neglected. Moreover, the refined energy balance provides the
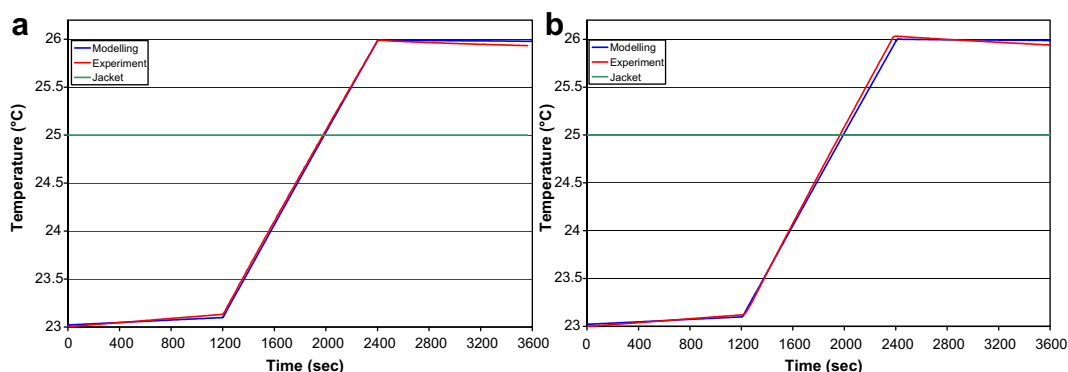

Fig. 8. Comparison between simulations and experiment of mean water bath temperature for calibration (a) and combustion (b) modes.
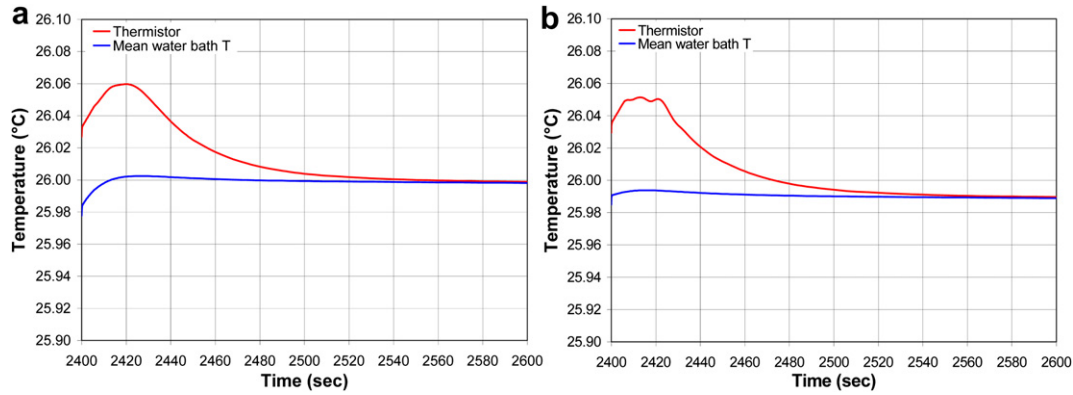
Fig. 9. Evolutions of the water bath temperature in the final period: (a) Combustion. (b) Calibration.

total radiative power, estimated to 2 W and represents less than 5% of the GCV [12]. However, the effect of this absence in the modelling can be seen here in Fig. 8b with a higher experimental temperature rise due to the radiative part of the burned gases in the burner.

5.3. Thermistor location

The temperature sensor (a 10 kΩ thermistor) is located between the burner and the vessel wall at the opposite side of the stirrer, at approximately 7 cm from the bottom [8]. The validation of the location in the bath was rechecked by new results from the refined geometric and thermal model. Fig. 9 exposes the evolutions of the mean bath temperature and the thermistor temperature for combustion (a) and for calibration (b) in the final period.

Temperature of the thermistor located at its initial position remains in the mean temperature range (mean water bath temperature ± 0.05 K). The sensitivity of the sensor is visible just at the maximum temperature where the water bath is thermally non-homogeneous and totally unstable (Fig. 9). In effect, at this time, the stored energy remained in burner glass is released to the bath and the final cooling period begins to happen.

Moreover, we can observe the light shift of maximum temperature times (see Table 2) from calibration to combustion due to the energy released by the hot gases remained in the burner (12 s in calibration and 28 s in combustion).

An experimental validation of the thermistor location was performed with a thermal characterisation of the water bath by the means of 18 thermistors located on a non-disturbing plastic holder. Fig. 10 presents the integration scheme of these sensors in the bath all around the burner. Probes numbered 1 to 6 are positioned to the bottom level in the bath (called level 1 in Fig. 10), 7 to 12 are located in the middle level (level 2) and sensors from 13 to 18 at the top level (level 3). The stirrer is schematised in Fig. 10.

The sensitivity and the resistance of the thermistors are identical to the probe used for experiments but they have been inserted without disturbing the homogenisation system. Temperature measurements were performed in combustion and electrical calibration. Thermistor 1 is at the same location as the probe used for all the experiments. We compared the mean temperature evolution with thermistor 1 to confirm the choice of this position. Fig. 11a presents a part of the initial period of a calibration run. The standard deviation of both initial and final periods is 14 mK and 20 mK in the heating period but the value for thermistor 1 is only 0.9 mK compared to the mean temperature (Fig. 11b).

Moreover, the temperature measurements issued from the thermal characterisation validated the combustion modelling in

the burner and especially the earlier remark (part 4.1) on the hot spot held at the top of the burner during combustion. Actually, the maximum temperatures have been always identified at the upper level (top of the burner), essentially at the site of sensors 18 and 14.

5.4. Temperature of the isothermal jacket

The mean water bath temperature was modelled in the calibration mode for two different jacket temperatures: 26.9 °C and 24.5 °C representing respectively a high and median jacket temperature.

Table 3 exposes a substantial increasing of the external energy from inwards the calorimeter with a jacket temperature of 26.9 °C. In that case and because the water bath temperature is always below that of the jacket, whatever the period, the jacket gives to the calorimeter a total amount energy of 3861 J (almost 7% on a total heating energy of 55836 J). Whereas in the other case, the
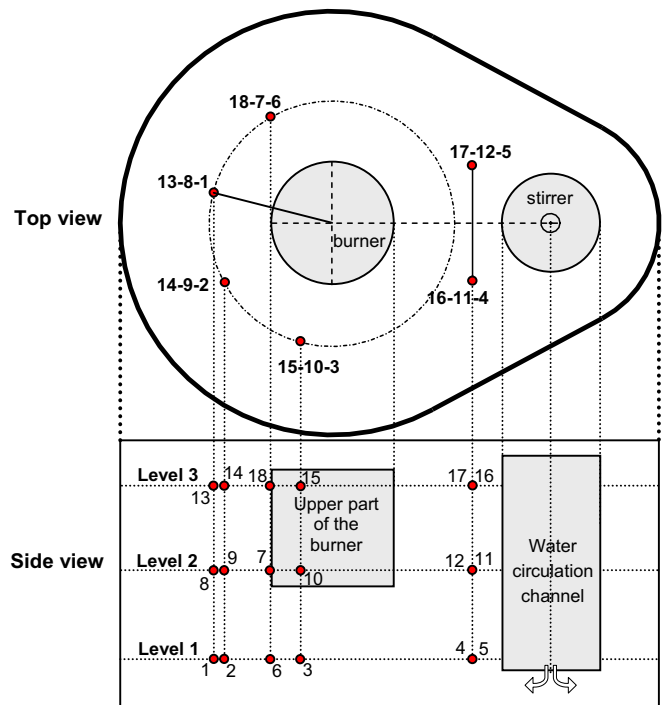

Fig. 10. Sketch of the calorimeter (top and side views) integrating the 18 thermistors, identified by numbers from 1 to 18. Axial and lateral representation of the bath allow for each sensor to be localized around the burner.
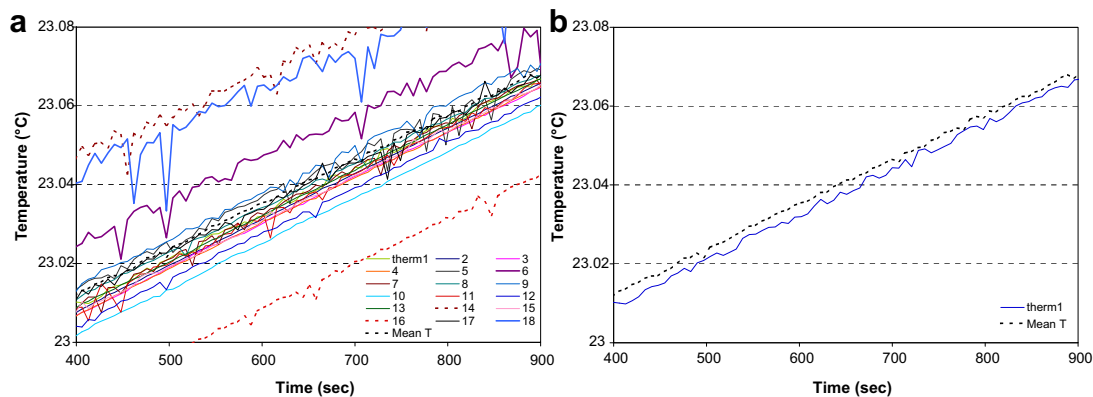
Fig. 11. Temperature-time curves in the first stable period (initial period) during 500 s for a calibration run. (a) of 18 thermistors located around the burner in the water bath (b) of the mean temperature and thermistor numbered 1.

Table 3
Energy received by the calorimeter can from the jacket bath for each period.

	Energy exchanged between the isothermal jacket and the calorimeter can (J)	
	T jacket = 26.9 °C	T jacket = 24.5 °C
Initial period	2162	860
Main period	1316	53
Final period	383	−843
Total	**3861**	**70**

energy exchanged from the jacket to the calorimeter can does not exceed 100 J.

6. Conclusion

An optimised modelling was performed by the R&D Division of GDF-Suez to reproduce with a high level of accuracy the different thermal heat fluxes transferred to the calorimetric water bath. The energy balance of the whole calorimetric system including the precise distributions between each part of the calorimeter was produced and exposes that in both modes (combustion and electrical heating), approximately 90% of the total energy is absorbed by the water bath and 10% by the calorimetric walls. The combustion mode was accurately reproduced by means of the complete simulation of the combustion in the burner, using the CFD and an advanced combustion model that uses the thermo kinetics database from reference flames calculations. The precise heat release of the flame was quantified accompanied by calculations of the burned gases temperatures.

A comparison study by numerical simulations showed a satisfied similarity between the calibration and the combustion mode. The numerical model fits quite closely with the experimental thermal behaviour of the calorimeter during electrical and combustion heating. Moreover, the experimentally observed dynamic and steady regimes were well represented by the modelling.

The temperature of the isothermal jacket fixed at 25 °C and the location of the temperature sensor representing the average water temperature were chosen according to the numerical simulations results.

The expected outcome of both experiments and thermal modelling will decrease the uncertainty of the calorific value measurements.

References

[1] Natural Gas − Calculation of Calorific Values, Density, Relative Density and Wobbe Index from Composition ISO 6976, International Organization for Standardization, Geneva, 1995.
[2] F.D. Rossini, The heat of formation of water, NBS, J. Res. 6 (1931) 1−35.
[3] F.D. Rossini, The heat of combustion of methane and carbon monoxide, NBS, J. Res. 6 (1931) 37−49.
[4] F.D. Rossini, The heat of formation of water and the heats of combustion of methane and carbon monoxide. A correction, NBS, J. Res. 7 (1931) 329−330.
[5] F.D. Rossini, Calorimetric determination of the heats of combustion of ethane, propane, n-butane and n-pentane, NBS, J. Res. 12 (1934) 735−750.
[6] F.D. Rossini, The heats of combustion of methyl and ethyl alcohols, NBS, J. Res. vol. 8 (1932) 119−139.
[7] C. Villermaux, M. Zaréa, F. Haloua, B. Hay, J.-R. Filtz, Measurements of gas calorific value: a new frontier to be reached with an optimised reference gas calorimeter, 23rd WGC (world gas conference), Amsterdam, 2006.
[8] F. Haloua, C. Villermaux, J.-R. Filtz, M. Zaréa, B. Hay, Thermal characterisation of an isoperibolic calorimeter bath, 9th TEMPMEKO conference (International Symposium on temperature and thermal measurements in Industry and Science), Dubrovnik, 2004.
[9] F. Haloua, B. Hay, J.-R. Filtz, New French reference calorimeter for gas calorific value measurements, J. Ther. Anal. Cal. 97 (2) (2009) 673−678.
[10] F. Haloua, Développement d'un calorimètre de référence pour la mesure du pouvoir calorifique des composants du gaz naturel avec une incertitude de ±0,05 %, Rapport final COPRU, 2002.
[11] C. Villermaux, M. Zaréa, Calorimètre de référence: simulation numérique de l'évolution de la température du bain, M.DU.IND.2005.0129.Cvi-KT, GDF-Suez internal report, 2005.
[12] J.-N. Ponsard, G. Lartigue, Simulations numériques 3D des écoulements et des transferts thermiques en régime transitoire du calorimètre du LNE, M.DU.IND.2007.0235.JNPo.KT, GDF-Suez internal report, 2007.
[13] B. Fiorina, O. Gicquel, S. Carpentier, N. Darabiha, Validation of the FPI chemistry reduction method for diluted non-adiabatic premixed flames, Comb. Sc. Tech. 176 (5−6) (2004) 785−797.
[14] J. Taine, J.-P. Petit, Transferts thermiques: Mécanique des fluides anisothermes, ed. Dunod, 1995.
[15] A. Pramann, Development of a reference gas calorimeter: final internal Report − project Part 1, Physikalisch-Technische Bundesanstalt, 2005.
[16] P. Borrell, The application of computer curve fitting techniques to Regnault-Pfaundler calculations of calorimetric data, Thermochim. Acta 9 (1974) 89−93.